Journal of Engineering Physics and Thermophysics, Vol. 81, No. 3, 2008

NEW POSSIBILITIES OF INVESTIGATING BLOOD FLOW IN SOFT TISSUES OF THE MOUTH

N. A. Fomin,[a] S. P. Rubnikovich,[b] and N. B. Bazylev[a]

UDC 616.31–07+681.787

It has been shown that the method of digital dynamic photography is an effective technique for quantitative and qualitative diagnosis of the microcirculatory state of mouth tissues. As a result of the signal processing, one can obtain information on microcirculation indices from the spectral distribution of low-frequency variations of the speckle structure. The investigated method of digital dynamic speckle photography can be used to elucidate the haemodynamic features in tissues of the oral cavity even at early stages of the disease and then at the examination and treatment stages. New possibilities of digital laser speckle technologies for tomographic investigations of the near-surface blood flow at various depths with the use of two-lens optical configurations are illustrated.

Introduction. The microcirculation system is the main link providing homeostasis in organs and tissues. Taking into account that the microvessels are the most sensitive indicators responding to pathogenic factors before the appearance of clinical inflammation symptoms in the parodontium, specialists think that the leading role in the development of pathology in the gum tissues is played exactly by this link of the vascular system [1–4]. In studying the state of the vascular system of the maxillofacial region, the following methods of functional diagnosis have found the widest use: rheoparodontography, polarography, contact biomicrography, and dopplerography. Their application makes it possible to make a diagnosis of the functional and structural changes in vessels and a preliminary forecast of the course of a disease. For instance, the method of contact biomicroscopy permits qualitative observation of the functional state of mucous membrane vessels and recording some of their parameters in analyzing the images obtained. Rheoparodontography is also a contact method and records changes in the electrical resistance of parodontium tissues when a low-frequency ac current (40–200 Hz) is passed through it. The closest to the contactless method of quantitative diagnosis of the near-surface blood flow intensity described in the present paper is dopplerography. Both optical and ultrasound dopplerographies are based on the effect of the change in the frequency of the scattered signal from a moving scatterer, a blood erythrocyte in the given case [5]. Such methods permit obtaining quantitative information only at individual points of the flow, and obtaining a complete flow pattern required scanning of the tissue by probe radiation. At the same time, in the last few years qualitative methods of flow visualization have been developed; they permit simultaneous obtaining of required information throughout the field without using scanning systems. These methods rely on the analysis of the dynamic behavior of speckle fields formed in the laser probing of biotissues. The rapid development of this direction in the last two decades was stimulated by advances in the laser field and digital technologies of coherent image input into a PC with the use of high-resolution CCD cameras in combination with the experience of accumulation of huge experimental data files in digital form and their statistical analysis immediately on the PC used for image storage. Such methods of investigation received the name digital dynamic speckle photography [6–9]. In the present paper, the principles of such methods are described, their possibilities are illustrated, and new optical schemes of speckle tomographs that permit differentiating the blood flow in biotissues at different depths are proposed.

Bio-Speckle Field Formation. Let us consider the processes of bio-speckle field formation in probing skin tissue by laser radiation. Schematically, skin tissue consists of three main parts: epidermis, dermis, and hypodermis

[a]A. V. Luikov Heat and Mass Transfer Institute, National Academy of Sciences of Belarus, 15 P. Brovka Str., Minsk, 220072, Belarus; email: fomin@hmti.ac.by; [b]Belarusian Medical State University, 83 Dzerzhinskii Ave., Minsk, 220116, Belarus. Translated from Inzhenerno-Fizicheskii Zhurnal, Vol. 81, No. 3, pp. 508–517, May–June, 2008. Original article submitted October 8, 2007.

1062-0125/08/8103-0533

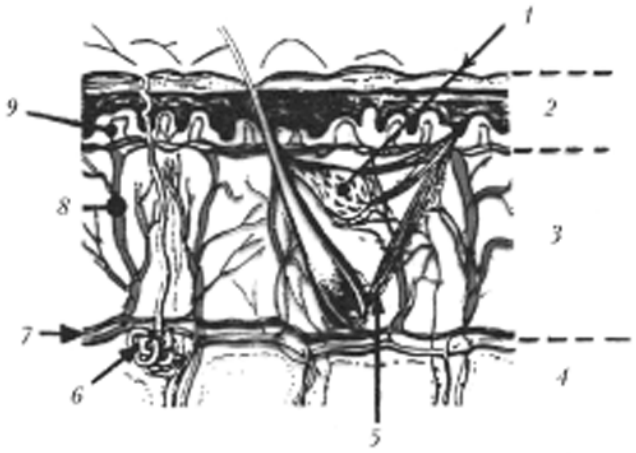

Fig. 1. Basic elements of human skin tissue: 1) oil gland; 2) epidermis; 3) dermis; 4) hypodermis; 5) arrector (muscle); 6) sweat gland; 7) nerve plexus; 8) blood vessel; 9) hypodermic capillary.

TABLE 1. Coefficients of Absorption κ and Scattering ε for Tissue and Blood at Various Radiation Wavelengths (according to the V. V. Barun and A. P. Ivanov model [11])

λ, nm	Tissue		Blood	
	κ_1	ε_1	κ_2	ε_2
400	2.32	105	857	10
450	1.22	70.9	286	7.85
500	0.7	50.6	100	7.43
550	0.46	37.8	200	8.57
600	0.345	29.4	12	8.93
650	0.29	23.6	2.07	9
700	0.266	19.4	1.43	8.57
750	0.254	16.3	1.7	8.1
800	0.249	14	3.15	7.6
850	0.248	12.1	3.9	7.27

(Fig. 1). Inside there are also sweat glands and apocrine glands which only exist in some parts of the human body. The arterial and venous circulation ends in the so-called "candelabra" — microcapillaries in subcutaneous papillae and numerous networks around the epiderma [10].

The laser radiation distribution in the biotissue can be estimated on the basis of the model developed under the supervision of Prof. A. P. Ivanov [11]. In the first approximation the attenuation coefficient of the laser radiation κ in the biotissue can be approximated as follows: $\kappa = (1 - C_v)\kappa_1 + C_v\kappa_2$. The scattering coefficient ε is expressed in the given model in a similar way: $\varepsilon = (1 - C_v)\varepsilon_1 + C_v\varepsilon_2$. The values of these coefficients for some probe radiation wavelengths, according to the data of [11], are given in Table 1.

Let us estimate the depths of penetration of the probe laser radiation into a blood-filled tissue. The depth dependence of the laser radiation intensity I is given by the formula $I = I_0 \exp(-\kappa l)$. Taking into account the data in Table 1, we have performed calculations of the laser radiation absorption in the tissue for two wavelengths: 550 and 650 nm at a different volume fraction of the blood filling the biotissue. The results of the calculations are given in Fig. 2.

The estimates presented show that the depth of penetration of the laser radiation into the biotissue largely depends on the degree of its filling with blood. For the helium-neon laser radiation the penetration depth can reach 300–600 μm or more, which is in good agreement with numerous experimental data [5, 6, 12, 13]. Thus, the laser radiation penetrates into the biotissue to a depth sufficient for probing the near-surface blood flow.

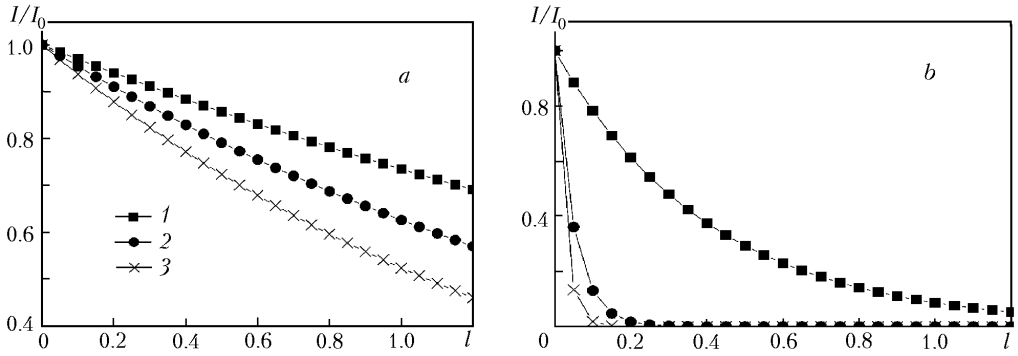

Fig. 2. Results of the calculations of the laser radiation absorption in the tissue for wavelengths of 550 nm (a) and 650 nm (b): 1) C_v = 0.01; 2) 0.1; 3) 0.2.

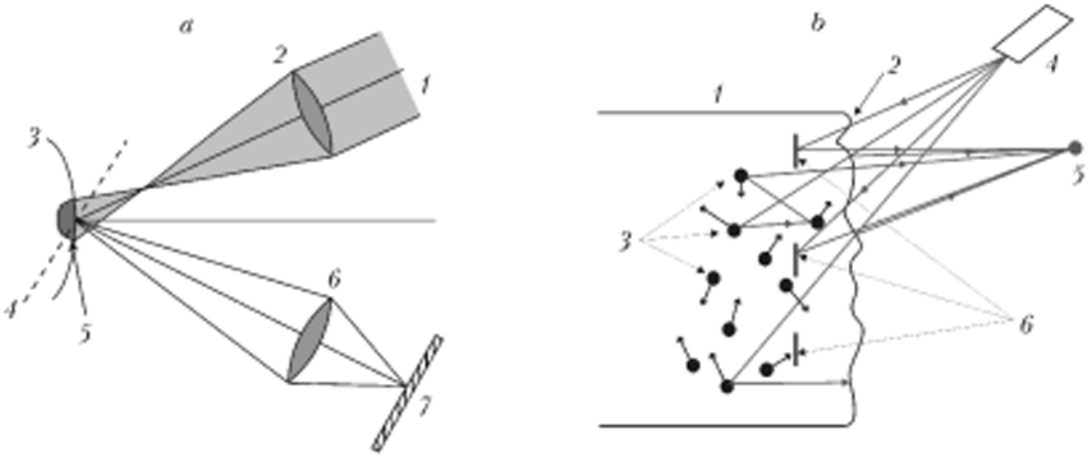

Fig. 3. Illumination geometry in probing a living tissue by laser radiation (a) [1) Gaussian beam; 2) lens; 3) *in vivo* biotissue; 4) recording plane of a speckle field; 5) illuminated volume; 6) lens II; 7) observation plane] and mechanism of speckle field formation in probing a biotissue (b) [1) biotissue model; 2) biotissue surface; 3) moving scatterers (blood erythrocytes); 4) probe laser; 5) formed speckle; 6) stationary scatterers in the biotissue].

Bio-speckle fields used to diagnose the transfer process in biotissues are generated in the processes of multiple scattering of coherent (laser) probe radiation by biotissue elements. In investigating the near-surface blood flow, the basic scattering elements are blood erythrocytes moving along the microcapillaries of the biotissues. As a consequence of this motion, the generated speckle field undergoes complex changes whose analysis permits obtaining information on the investigated processes. The statistical description of the dynamics of change in the speckle field will be carried out below with the use of space-time correlation functions describing the correlation of the scattered probe radiation intensity at different points in space and at different instants of time. A speckle field is formed in the biotissue-scattered radiation as a result of the coherent addition of the amplitudes of the light waves that arrive at a given point in space with different phases as a result of the processes of multiple scattering in the probed medium and, as for other random media, can be described in the random walk model [14] (Fig. 3). A convenient model of the static speckle field formation is the laser radiation scattering by a diffuse rough surface. Under "ideal" conditions of speckle field formation it is assumed that the diffuse surface microasperities obey Gaussian statistics with a value of rms deviation much larger than the probe radiation wavelength. The coherent length of the laser and the size of the irradiated zone thereby should be much greater than the optical path difference for all beams that arrive at the observation point. As the scatterers are moving, the speckle field also begins to move and its correlation function becomes time-dependent.

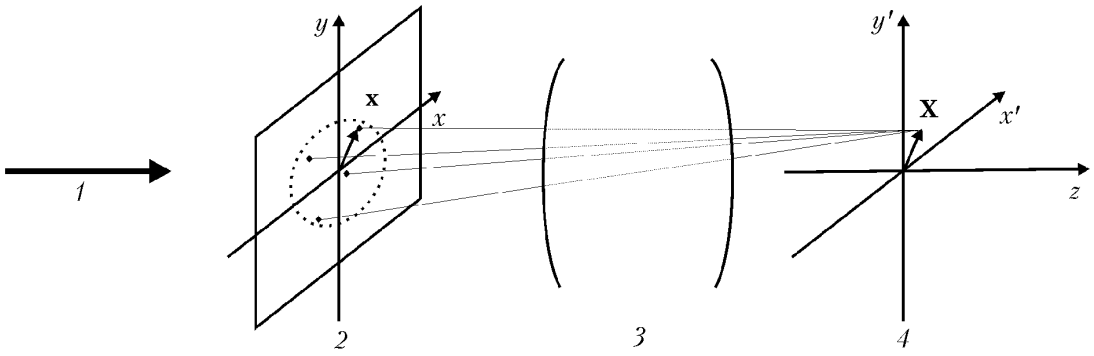

Fig. 4. General geometry of speckle field formation from a moving diffuse object by means of a linear optical system: 1) coherent illumination; 2) scattering plane; 3) imaging optical system; 4) image plane.

In biotissues and, accordingly, in speckle fields the processes of multiple scattering are complicated by the fact that the act of scattering by particles moving with different velocities can occur [15].

Two methods for changing speckle fields are distinguished. These are "shifting" of the speckle field at which some aggregate of speckles shifts as a unit without changing their relative position, and "boiling" of speckles when individual speckles appear and disappear chaotically at the same points in space without experiencing noticeable shifts. Two parameters — the correlation time τ_c and the delay time τ_d — were introduced in [7] to describe the dynamic properties of speckle fields experiencing simultaneously two modes of change: "shifting" and "boiling":

$$\gamma_{\Delta I}(\mathbf{r}, \tau) = \exp\left(-\frac{|\mathbf{r}|^2}{r_c^2}\right)\exp\left[-\frac{(\tau - \tau_d)^2}{\tau_c^2}\right], \tag{1}$$

where $\mathbf{r} = \mathbf{r}_2 - \mathbf{r}_1$; $\tau = t_2 - t_1$; the delay time τ_d depends on $\mathbf{r}$.

Formation of Bio-Speckle Fields in More Complex Configurations. A speckle field is formed in scattered light as a result of the interference of all beams incident on a given point. As a rule, in recording speckle fields one uses different optical systems which also influence the field characteristics (Fig. 4). It is supposed that by virtue of the diffusivity of a biological object the phase differences of all beams forming a speckle field are uniformly distributed in the 0–2π range. Let $\mathbf{x} = \mathbf{x}(x, y)$ be Cartesian coordinates in the object plane and $\mathbf{X} = \mathbf{X}(x', y')$ coordinates in the image (observation) plane (Figs. 4–7). When a diffuse object is illuminated by a stationary light wave having a complex amplitude $\mathbf{E}_0 = \mathbf{E}_0(x)$, the complex amplitude of the scattered wave in the recording plane will be defined by the transfer function of the optical system $\mathbf{K} = \mathbf{K}(\mathbf{x}, \mathbf{X})$:

$$\mathbf{E}(\mathbf{X}, t) = \int \mathbf{E}_0(\mathbf{X}, t) \times \mathbf{K}(\mathbf{x}, \mathbf{X})\, dx\,. \tag{2}$$

To simplify the recording, let us introduce one-dimensional transfer functions of the optical system $r_i = |\mathbf{K}(0, \mathbf{X})|^2$ and $r_0 = |\mathbf{K}(0, \mathbf{X})|^2$ (Table 2). For the lensless geometry (Fig. 5), we represent the full transfer function as

$$\mathbf{K}(\mathbf{x}, \mathbf{X}) = \frac{k}{i2\pi l}\exp\left(ik\frac{|\mathbf{x} - \mathbf{X}|^2}{2l}\right)\exp(ikl)\,. \tag{3}$$

For the optical configuration with one lens this function is written in the form

$$\mathbf{K}(\mathbf{x}, \mathbf{X}) = \frac{-k^2q^2}{4\pi i l_1 l_2}\exp\left[\frac{-k^2q^2}{4(1+\theta_1^2)}\left|\frac{\mathbf{x}}{l_1} - \frac{\mathbf{X}}{l_2}\right|^2\right]\exp\left\{i\left[k\left(l_1 + l_2 + \frac{|\mathbf{x}|^2}{2l_1} + \frac{|\mathbf{X}|^2}{2l_2}\right)\right.\right.$$

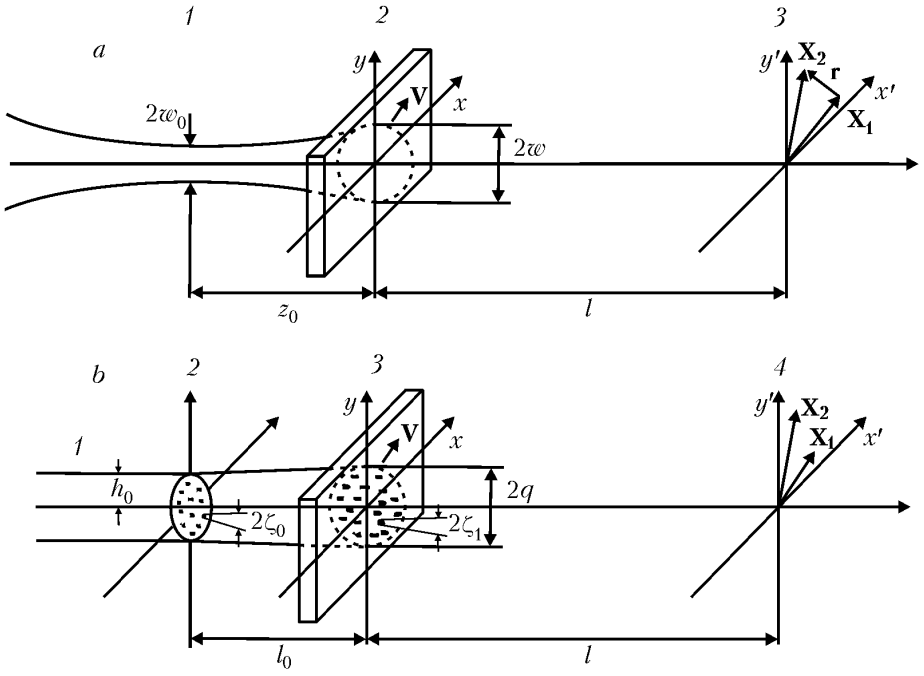

Fig. 5. Formation of a dynamic speckle field due to the radiation scattering by a biotissue, in which the scatterers move with velocity **V**(*x*, *y*), in probing the biotissue by a laser source with Gauss intensity distribution (a) [1) Gaussian beam; 2) biotissue; 3) image plane] and "restricted" Gaussian distribution (b) [1) optical fibre; 2) source plane; 3) biotissue; 4) image plane].

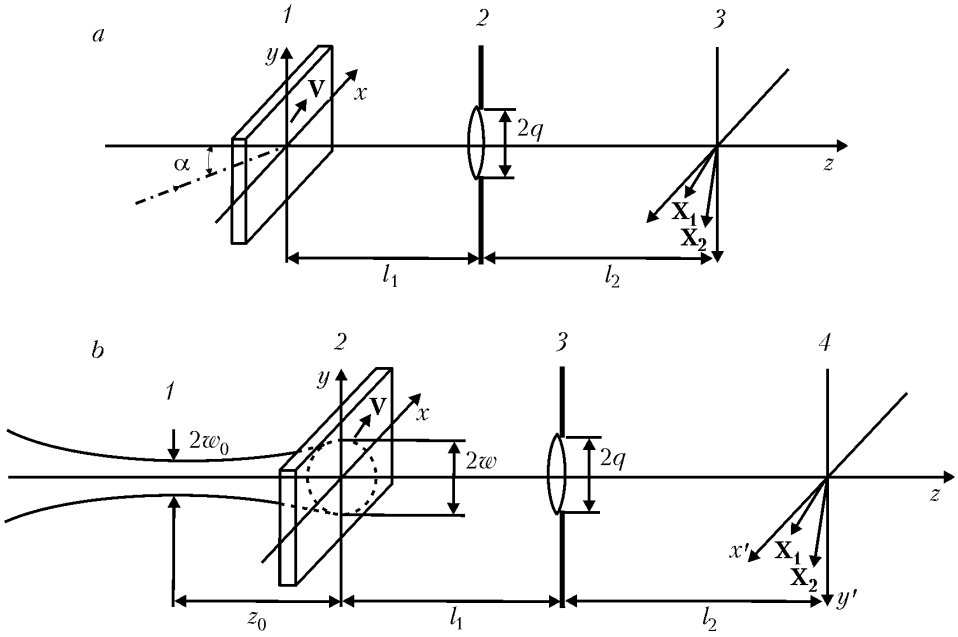

Fig. 6. Formation of a dynamic speckle field due to the radiation scattering by a biotissue, in which the scatterers move with velocity **V**(*x, y*), by means of a single-lens optical system in probing the biotissue by a collimated laser source (a) [1) biotissue; 2) lens plane; 3) image plane] and by a laser source with a Gauss intensity distribution (b) [1) Gaussian beam; 2) biotissue; 3) lens plane; 4) image plane].

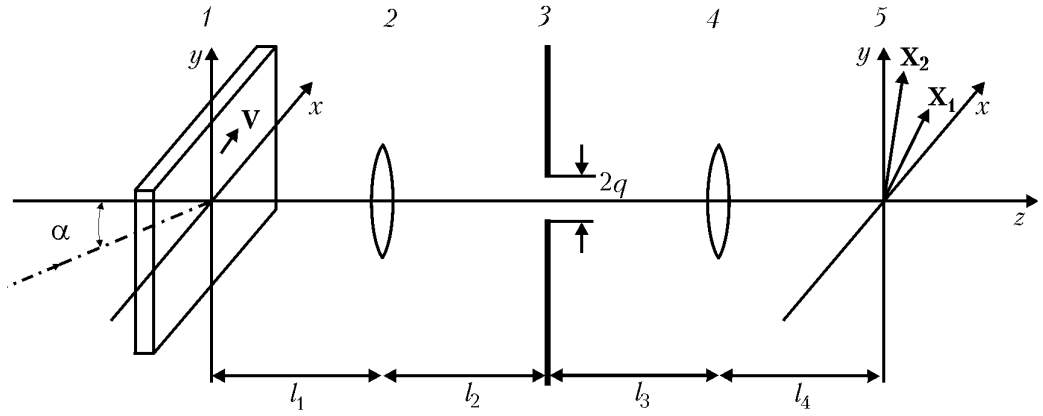

Fig. 7. Formation of a dynamic speckle field due to the radiation scattering by a biotissue, in which the scatterers move with velocity $\mathbf{V}(x, y)$, by means of a two-lens optical system in probing the biotissue by a collimated laser source: [1) biotissue; 2) plane of lens I; 3) diaphragm plane; 4) plane of lens II; 5) image plane.

TABLE 2. Average Size of Speckles r_s and Transfer Functions of the Optical System r_0 and r_i for Various Optical Configurations

Optical configuration	Parameters of the optical system		
	r_s	r_0	r_i
Fig. 5a	$\frac{2l}{k_0 w}$	—	—
Fig. 5b	$\frac{l}{l_0}\zeta_0$	—	—
Fig. 6a	$\frac{2l_2}{k_0 q}$	$\frac{1}{2}r_s(1+\theta_1^2)^{1/2}$	$\frac{l_1}{k_0 q}(1+\theta_1^2)^{1/2}$
Fig. 6b	$\frac{2l_2}{k_0 q}$	$\frac{1}{2}r_s(1+\theta_1^2)^{1/2}$	$\frac{l_1}{k_0 q}(1+\theta_1^2)^{1/2}$
Fig. 7	$\frac{2}{k_0 k}\left(l_3+l_4-\frac{l_3 l_4}{F_2}\right)$	$\frac{1}{2}r_s(1+\theta_2^2)^{1/2}$	$\frac{l_1 l_2 A_1}{k_0 q}(1+\theta_2^2)^{1/2}$
Fig. 7, $l_2 = F_1$, $l_3 = F_2$	$\frac{2F_2}{k_0 q}$	$\frac{1}{2}r_s(1+\theta_2^2)^{1/2}$	$\frac{F}{k_0 q}(1+\theta_2^2)^{1/2}$

$$+\tan^{-1}\theta_1 - \frac{k^2 q^2 \theta_1}{4\,(1+\theta_1^2)}\left|\frac{\mathbf{x}}{l_1}-\frac{\mathbf{X}}{l_2}\right|^2\Bigg]\Bigg\}. \tag{4}$$

The parameters l_1, l_2, q are shown in Fig. 6, and $\theta_1 = \frac{kq^2}{2}\left(\frac{1}{l_1}+\frac{1}{l_2}-\frac{1}{F}\right)$. For a more complex imaging system consisting of two lenses (Fig. 7), the transfer function has the form

$$\mathbf{K}(\mathbf{x}, \mathbf{X}) = \frac{-k^2 q^2}{4\pi i l_1 l_2 l_3 l_4 A_1 A_2 (1+\theta_2^2)^{1/2}} \exp\left[\frac{-k^2 q^2}{4\,(1+\theta_2^2)}\left|\frac{\mathbf{x}}{A_1 l_1 l_2}-\frac{\mathbf{X}}{A_2 l_3 l_4}\right|^2\right]$$

$$\times \exp\left\{ i\left[k\left(l_1 + l_2 + l_3 + l_4 + i\tan^{-1}\theta_2\right) + i\frac{k}{2}\left[\frac{1}{l_1}\left(1 - \frac{1}{A_1 l_1}\right)|\mathbf{x}|^2 + \frac{1}{l_4}\left(1 - \frac{1}{A_2 l_4}\right)|\mathbf{X}|^2\right]\right.\right.$$

$$\left.\left. - i\frac{k^2 q^2 \theta_2^2}{4\left(1 + \theta_2^2\right)}\left|\frac{\mathbf{x}}{A_1 l_1 l_2} + \frac{\mathbf{X}}{A_2 l_3 l_4}\right|^2\right]\right\}. \tag{5}$$

Here $A_1 = \frac{1}{l_1} + \frac{1}{l_2} - \frac{1}{F_1}$; $A_2 = \frac{1}{l_3} + \frac{1}{l_4} - \frac{1}{F_2}$; $\theta_2 = \frac{kq^2}{2}\left(\frac{1}{l_2} - \frac{1}{A_1 l_2^2} + \frac{1}{l_3} - \frac{1}{A_2 l_3^2}\right)$.

Table 2 gives the basic relations for the dynamic speckle fields in the optical configurations presented in 5–7.

Experimental. The results of the first observations of the speckle fields obtained under radiation scattering from biological objects were published as long ago as in 1975 [16, 17]. J. D. Briers noted that the speckle field generated by radiation scattering from tomatoes fluctuates [17]. The degree of fluctuation was estimated proceeding from the contrast of the speckle field recorded on a photographic film with an exposure of 1.5 sec. These time fluctuations of the speckle field were caused by the chaotic motion of plastids or mineral particles in tomato cells. At the same time M. D. Stern observed speckle fields formed by laser radiation scattered from living tissue [16]. He noticed that speckle fields can be used to visualize the blood flow and conducted the first experiments with Doppler blood flow meters.

In our experiments, we chose as the radiation source a small-size semiconductor laser lasing at a wavelength of 680 nm and matched to a polymer optical fiber. The scheme allowed for the variation of the laser radiation power over a wide range, as well as for precision adjustment of the working point of both the optical and the electronic parts of the scheme. The speckle field obtained was recorded by a JAI Corp. (Japan) CCD camera. The CCD camera contains sensitive cells (in the amount of 768 × 494) located on a matrix of size 6.45 × 4.84 mm. In using this CCD camera, the time of exposure can be varied from 1/60 sec to 10 μsec. The recording frequency is 25 frames per second. The signal from the CCD camera arrives at an A to D converter and the PC chart having its own memory of size 2 MB. In digital recording of the field by means of the CCD matrix, the laser radiation intensity can be given in the matrix form $I(p', q')$, and the contrast value can be determined by direct calculation in each averaging window (m, n) by the formula

$$\mathbb{C}(m,n) = \frac{\sigma_1(m,n)}{\langle I(m,n)\rangle} = \frac{\sqrt{\langle I(m,n)^2\rangle - \langle I(m,n)\rangle^2}}{\langle I(m,n)\rangle}$$

$$= \frac{\sqrt{\frac{1}{MN}\sum_{p'=1}^{M}\sum_{q'=1}^{N}\left[I^{m,n}(p',q')\right]^2 - \left[\frac{1}{MN}\sum_{p'=1}^{M}\sum_{q'=1}^{N} I^{m,n}(p',q')\right]^2}}{\frac{1}{MN}\sum_{p'=1}^{M}\sum_{q'=1}^{N} I^{m,n}(p',q')}. \tag{6}$$

In a perfect speckle field the σ_1 value is equal to the mean intensity of the field $\sigma_1(m, n) = \langle I(m, n)\rangle$, and the contrast therewith is $\mathbb{C}(m, n) = 1$. If this statistics is disturbed, e.g., due to a change in the microstructure of the investigated specimen, the field contrast changes and the microstructure modification can be characterized quantitatively by the value of changes in the contrast.

Spatial Resolution of the Method. In the recording plane, it is determined by the receiving matrix parameters and the sizes of the so-called averaging windows (zones) by which primary statistical analysis of measurement data is performed. Qualitative processing of specklograms requires comparatively large averaging windows, especially for cross-correlation analysis of images at large shifts between exposures. The analysis performed shows that the rms error in determining the shift of the speckle field decreases 2–3 times as the window size increases from 32^2 to

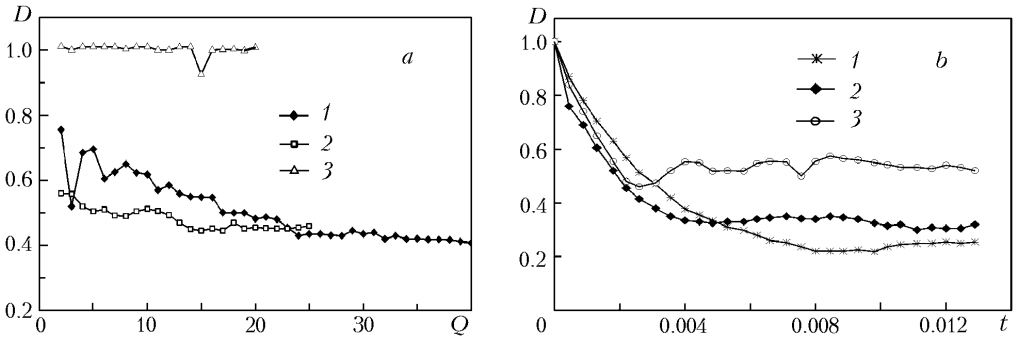

Fig. 8. Change in the structural function D with time for various biotissues (a) [1) *in vivo* blood flow; 2) apple pulp; 3) concrete (for control)] and portions of human skin (on the hand) with a different blood flow intensity (b) [1) high; 2) medium; 3) low].

128^2. Such an increase in the size of averaging windows inevitably leads to considerable losses in the spatial resolution. Accordingly, as the window size decreases from 32^2 to 16^2, the losses increase 2–3 times, but can still be minimized to values of the order of 0.1 of the pixel size d_{px} upon optimization of all the other parameters of measurements. The use of such a window for a Fuji FinePixS2Pro matrix at optical magnification $\mathfrak{M} = 1$ and with covering 0.5 of the window provides a limiting spatial resolution of the order of 50 μm throughout a 20×30 mm^2 field. A further decrease in the window size without loss of accuracy of the statistical processes is only possible in special cases. For instance, in particular, for autocorrelation analysis in the single-exposure scheme the window size can be even smaller, down to 5×5 or 7×7 pixels [12, 18, 19].

Temporal Resolution. In recording velocity fields, it is determined by both the measuring circuit and the technical characteristics of the camera and processor. In using a *two-exposure* scheme, the velocity field is determined as a result of the statistical analysis of the shifts of scatterers in the time interval between sequential frames obtained for exposures shorter than the characteristic time of the investigated flow. In this case, the temporal resolution is determined by the minimal time interval between sequential frames, and in realizing continuous monitoring of the velocity, it is determined by the frequency of repetition of recording pairs of images and the time of the cross-correlation analysis on the PC. The *single-exposure* technique uses a prolonged exposure during which the particles noticeably shift in the plane, and the autocorrelation analysis of these images makes it possible to determine the shift value in the time of exposure. In this case, the temporal resolution of this technique is determined by the minimal time of exposure, which is much shorter than the time interval between sequential frames. In investigating ultrafast processes, the temporal resolution in this scheme can be increased to an even greater extent by recording with an open shutter of the camera and controlling the exposure by controlling the duration of the laser radiation. And the exposure time in using the shutter of the given CCD camera can be varied from a few seconds to 250 μsec.

The application of the so-called structural function widely used in describing turbulent flows

$$D_1(p', q') = \frac{MN}{(M-p')(N-q')} \left[\frac{\sum\limits_{m=1}^{M-p'} \sum\limits_{n=1}^{N-q'} (I_1(m,n) - I_2(m+p', n+q'))^2}{\sum\limits_{m=1}^{M} \sum\limits_{n=1}^{N} I_1(m,n)\, I_2(m,n)} \right] \tag{7}$$

also turns out to be quite efficient. The experimental data (Fig. 8) point to the fact that in the dynamic speckle field generated by the surface blood flow very high frequencies, up to 1–2 kHz, are present. This places special demands on the recording equipment for complete reflection of the high-frequency region of the spectrum of the dynamic speckle field.

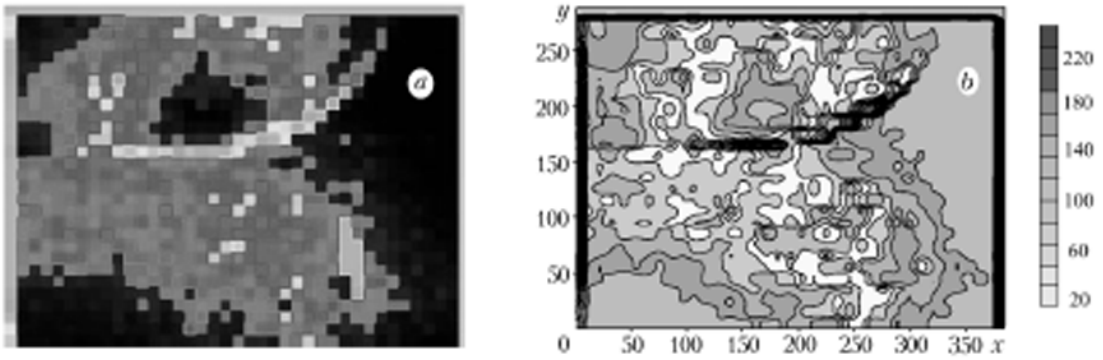

Fig. 9. Isolines of the speckle field contrast (a) and value of the near-surface blood flow in arbitrary units (b).

Such high-frequency processes can be visualized in the regimes of real or quasi-real time in the scheme of single-exposure speckle photography. In this case, each speckle field recorded by the CCD camera during a longer time comparable to the characteristic time of the investigated ultrafast process is analyzed. In such a recording, the image "blurs" and its contrast softens. In this connection, the contrast value of the time-integrated speckle field may serve as a characteristic of the averaged shift of speckles in the exposure time. The value of this contrast and the intensity values of the near-surface blood flow in the form of isolines obtained in real time are given in Fig. 9.

Note that the autocorrelation analysis is much simpler than the cross-correlation one, which permits increasing the frequency of real- or quasi-real-time output of processed information onto the monitor. This frequency can easily be increased to 25 Hz even using a medium-class PC. However, the chief advantage of the single-exposure technique is the possibility of a very large increase in the rate of change in the process being investigated. This rate in the given scheme is associated not with the time interval between sequential frames, but with the recording time of each image, which in standard CCD cameras can be varied from 10 μsec to 40 msec. Exactly this fact makes it possible, using the single-exposure technique, to investigate processes with characteristic frequencies up to 100 kHz and higher, which is more than enough for recording the dynamics of biospeckle fields.

Conclusions. The method of digital dynamic speckle photography gives local information simultaneously throughout the investigated zone and permits real-time analysis of the hemodynamics. As a result of the signal processing by the spectral distribution of low-frequency variations of the speckle structure, one can obtain information about microcirculation indices. The investigated method of digital dynamic speckle photography can be used to elucidate the features of the hemodynamics in mouth tissues even at early stages of the disease as well as at the examination and treatment stages.

The authors wish to thank Academician S. A. Zhdanok, Prof. S. A. Naumovich, and Dr. of Science (physics and mathematics) O. G. Penyaz'kov for support and helpful discussions, Candidates of Science E. I. Sakevich and P. P. Khramtsov for assistance in performing experiments and developing programs for mathematical treatment of images, as well as the Belarusian Republic Basic Research Foundation of the National Academy of Sciences of Belarus for partial financial support by grants and as part of the projects "Nanotech 1.13", "Thermal processes-25", T07-070, and T07M-112.

NOTATION

A_1, A_2, coefficients, m^{-1}; C_v, volume fraction of filling biotissue with blood; d_{px}, pixel size of the CCD matrix, μm; $D_I(p, q)$, structural function of the laser radiation intensity in the speckle field; $\mathbf{E}_0$, vector of the complex amplitude of the sounding wave, V; $\mathbf{E}(\mathbf{X}, t)$, vector of the complex amplitude of the wave in the speckle field, V; F_1, F_2, F_3, focal lengths of lenses, m (Figs. 6, 7); h_0, fiber radius, μm (Fig. 5b); i, imaginary unit; $I(m, n)$, $I(p, q)$, $I(p', q')$, laser radiation intensity in the speckle field, W/m^2; $\langle I(m, n)\rangle$, window-mean laser radiation intensity in the speckle field, W/m^2; k_0, k, wave number, cm^{-1}; $\mathbf{K}(\mathbf{x}, \mathbf{X})$, transfer function of the optical system; l, distances from the object and source planes to the image plane, m; l_1, l_2, l_3, l_4, geometric parameters (Figs. 6, 7); M, N, sizes of the dis-

cretization region in statistical processing; (m, n), current coordinates in the original image; (p', q'), cell number in the CCD matrix; q, imaging lens radius (Figs. 6, 7); Q, number of frames (Fig. 8a); $\mathbf{r}$, z, spatial coordinates, m; r_c, characteristic size of correlation in the speckle field, μm; r_s, mean size of speckles, μm; r_0, r_i, one-dimensional transfer functions of the optical system; t, time, sec; $\mathbf{V}(x, y)$, velocity of scatterers (Fig. 7), cm/sec; w and w_0, current radius of the laser beam and radius in its waist (in focus), m and mm; $\mathbf{x}$ and $\mathbf{X}$, vectors in the object and image plane, respectively, m; (x, y) and (x', y'), coordinates in the object and image plane, m; z_0, distance from the laser beam waist in focus to the biotissue (Fig. 5); α, angle of incidence of radiation, rad (Figs. 6, 7); $\gamma_{\Delta I}(\mathbf{r}, \tau)$, space-time correlation function of the laser radiation in the speckle field; ε_1 and ε_2, scattering coefficients of tissue and blood, respectively, cm^{-1}; ζ'_0 and ζ_1, radius of speckles in the plane of the source and a diffuse object, respectively, μm (Fig. 5b); θ_1 and θ_2, parameters (Figs. 6, 7); κ, attenuation coefficient of laser radiation, cm^{-1}; κ_1 and κ_2, absorption coefficient of laser radiation in tissue and blood, respectively, cm^{-1}; λ, laser radiation wavelength in the medium, μm; λ_0, laser radiation wavelength in vacuum, μm; σ_I, rms deviation of the laser radiation intensity in the subregion, W/m^2; τ, time interval, sec; τ_c, correlation time in the speckle field; τ_d, delay time in the speckle field; $\mathbb{C}(m, n)$, contrast of the speckle field; $\mathfrak{M}$, optical magnification in recording specklograms. Subscripts: c, correlation; d, delay; px, pixel; s, speckle; v, volume; 0, initial value of a physical quantity; 1, 2, 3, ..., ordinal values of physical quantities; $\langle ... \rangle$, mean value of a quantity.

REFERENCES

1. V. A. Kozlov, N. K. Artyushenko, O. V. Shalak, M. B. Girina, I. I. Girin, and E. A. Morozova, *Ultrasonic Dopplerography of the Macro- and Microcirculatory Channel Vessels of the Mouth*, *Face*, *and Neck Tissues* [in Russian], Minimaks, St. Petersburg (1999).
2. L. Yu. Orekhova, E. D. Kuchumova, O. V. Prokhorova, and T. B. Tkachenko, Evaluation of the parodontium microcirculation by the method of ultrasonic Dopplerography, *Parodontologiya*, **21**, No. 3, 21–24 (2001).
3. E. K. Krechina, *Disturbances of the Microcirculation in Bad Paradontium Tissues and Clinicofunctional Justification of the Methods of Their Correction*, Author's Abstract of Doctoral Dissertation (in Medicine), TsNII Stomatologii MZ RF (1996).
4. N. K. Loginova, *Functional Diagnostics in Stomatology* [in Russian], Partner, Moscow (1994).
5. P. Venneman and J. Westerweel, Full-field blood velocity measurement techniques, in: *Advanced Course and Workshop on Blood Flow*, BF 2005, Warsaw (2005), pp. 91–108.
6. Y. Aizu and T. Asakura, Bio-speckle phenomena and their applications to blood-flow measurements, in: *Proceedings of SPIE Conference on Time Resolved Spectroscopy and Imaging of Tissues*, **1431**, SPIE Press, Bellingham (1991), pp. 239–250.
7. T. Asakura and N. Takai, Dynamic laser speckle techniques and their application to velocity measurement of diffuse object, *J. Appl. Phys.*, **25**, 179–194 (1981).
8. N. Fomin, *Speckle Photography for Fluid Mechanics Measurements*, Springer Verlag, Berlin (1998).
9. N. B. Bazylev, S. M. Vlasenko, E. I. Lavinskaya, and N. A. Fomin, Quasi-real-time, Digital speckle photography of fast processes. *Dokl. Akad. Nauk Belarusi*, **45**, No. 5, 55–59 (2001).
10. A. Dittmar, J. Jossinet, E. McAdams, G. Delhomme, and J. Pigasse (Eds.), Innovation et Technologie en iologie et Medicine, *Proc. UETP/COMETT-BME Seminar*, Special Issue, **12** (1991).
11. V. V. Barun and A. P. Ivanov, Thermal action of a short light pulse on biological tissue, *Int. J. Heat Mass Transfer*, **46**, 3243–3254 (2003).
12. J. D. Briers, Laser speckle techniques in biology and medicine, in: *SPIE Proc.*, **2083**, Bellingham–Washington (1994), pp. 238–249.
13. N. Fomin, C. Fuentes, J.-B. Saulnier, and J.-L. Tuhault, Tissue blood flux monitoring by laser speckle photography, *Laser Physics*, **11**, No. 4, 525–529 (2001).
14. T. Okamoto and T. Asakura, The statistics of dynamic speckles, in: E. Wolf (Ed.), *Progress in Optics*, **34**, Amsterdam (1995), pp. 183–248.

15. N. B. Bazylev, E. I. Lavinskaya, S. A. Naumovich, S. P. Rubnikovich, and N. A. Fomin, Quasi-Real-Time Diagnostics of biotissues by the methods of laser probing and dynamic speckle photography, *Heat- and Mass Transfer–2003* [in Russian], A. V. Luikov ITMO NAN Belarusi, Minsk (2003), pp. 147–153.
16. M. D. Stern, In vivo evaluation of microcirculation by coherent light scattering, *Nature*, **254**, 56–58 (1975).
17. J. D. Briers, Wavelength dependence of intensity fluctuations in laser speckle pattern from biological specimens, *Opt. Communications*, **13**, 324–326 (1975).
18. A. M. Fercher and J. D. Briers, Flow visualization by means of single-exposure speckle photography, *Opt. Communications*, **37**, 326–330 (1981).
19. N. B. Bazylev, N. A. Fomin, E. I. Lavinskaya, and S. P. Rubnikovich, Real-time blood micro-circulation analysis in living tissues by dynamic speckle technique, in: *Proc. 13th Conf. European Society of Biomechanics* (*Acta of Bioengineering and Biomechanics*), 1–4 September 2002, Wroclaw, Poland (2002), Vol. 4, suppl. 1, pp. 510–511.